Accepted Manuscript

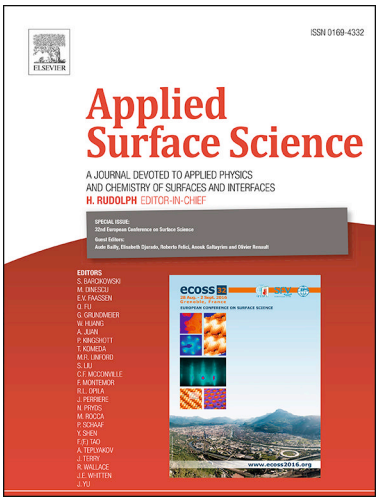


Full Length Article

# ZnO-Graphene Quantum Dots Heterojunctions for Natural Sunlight-driven Photocatalytic Environmental Remediation

Suneel Kumar, Ankita Dhiman, Pitchaimuthu Sudhagar, Venkata Krishnan

PII: S0169-4332(18)31000-6
DOI: https://doi.org/10.1016/j.apsusc.2018.04.045
Reference: APSUSC 39044

To appear in: *Applied Surface Science*

Received Date: 15 September 2017
Revised Date: 4 January 2018
Accepted Date: 5 April 2018

Please cite this article as: S. Kumar, A. Dhiman, P. Sudhagar, V. Krishnan, ZnO-Graphene Quantum Dots Heterojunctions for Natural Sunlight-driven Photocatalytic Environmental Remediation, *Applied Surface Science* (2018), doi: https://doi.org/10.1016/j.apsusc.2018.04.045

# ZnO-Graphene Quantum Dots Heterojunctions for Natural Sunlight-driven Photocatalytic Environmental Remediation

Suneel Kumar,[a] Ankita Dhiman,[a] Pitchaimuthu Sudhagar[b] and Venkata Krishnan[a]*

[a]*School of Basic Sciences and Advanced Materials Research Center, Indian Institute of Technology Mandi, Kamand, Mandi 175005, Himachal Pradesh, India.*

[b]*Multi-functional Photocatalyst & Coatings Lab, SPECIFIC, College of Engineering, Swansea University (Bay Campus) Swansea SA1 8EN, Wales, United Kingdom.*

** Corresponding author Email:* vkn@iitmandi.ac.in

## Abstract

In this work, we report the formation of heterojunctions comprising of graphene quantum dots (GQD) decorated ZnO nanorods (NR) and its use as efficient photocatalysts for environmental remediation. The heterojunctions has been designed to be active both in the UV and visible light regions and anticipated utilize the maximum part of the solar light spectrum. In this view, we examined the photocatalytic performance of our heterojunctions towards the degradation of colored pollutant (methylene blue (MB) dye) and a colorless pollutant (carbendazim (CZ) fungicide) under sunlight irradiation. Compared to bare photocatalyst ZnO and GQD, the heterojunction with 2 wt% of GQD (ZGQD2) showed the best photocatalytic activity by effectively degrading (about 95%) of organic pollutants (MB and CZ) from water within a short span of 70 min. The superior photocatalytic activity of these ZnO-GQD heterojunctions could be attributed to efficient charge carrier separation lead suppressed recombination rate at photocatalyst interfaces. In addition to the enhanced light absorption from UV to visible region, the high specific surface area of ZGQD2 heterojunction (353.447 $m^2 g^{-1}$) also imparts strong adsorption capacity for pollutants over catalyst surface, resulting in high photoactivity. Based on the obtained results, band gap alignment at ZnO-GQD heterojunction and active species trapping experiments, a plausible mechanism is proposed for photocatalytic reaction. The excellent photostability and recyclability of the ZnO-GQD heterojunctions fostering as promising photocatalyst candidate for environmental remediation applications.

**Keywords:** ZnO; graphene quantum dots; heterojunctions; charge transfer; photocatalysis; environmental remediation

## 1. Introduction

Over the past few decades, the demand of clean energy and pollution free environment (water and air) has increased worldwide due to rapid industrialization and population growth [1-3]. Different industries such as cosmetic, textile, paper, leather, pharmaceutical and fertilizer produces huge amount of pollutants in the water bodies, which are highly toxic and carcinogenic to human life even in trace concentration [4, 5]. Therefore, environmental friendly technique has to be developed to treat the water pollutant which does not produce further adverse effect to the environment. In this context, solar energy based water treatment has received much attention as is renewable, pollutant-free and abundance in nature [6]. Semiconductor based photocatalysis has emerged as economic, environmental benign technology because of its potential to solve the growing concerns of water pollution [7, 8] using sunlight irradiation. Nevertheless, photocatalytic performance of most of semiconductors have been limited for practical applications due to inadequate visible light utilization in solar spectrum, fast recombination of photoinduced charge carriers and thus affect the catalysis rate of pollutant degradation[9]. Therefore, to design the efficient photocatalytic materials which harvest high amount of light photons from solar energy spectrum, cost effective, and earth abundant is arduous task to scientific community. Among various semiconductors, $TiO_2$ and ZnO have been widely explored as promising materials for environmental remediation for the removal of organic pollutants from water [10-12]. In addition, carbon based material such as, graphitic carbon nitride (g-$C_3N_4$) has gained immense attention due unique optical, electrical and physiochemical properties and has been widely explored for energy generation and environmental remediation applications [13-16]. Owing to the simple synthesis routes, excellent chemical stability, non-toxicity and favorable band edge position for water oxidation, the metal oxide semiconductors have emerged as promising candidates for photocatalytic applications [17-19]. However ZnO has been considered as relatively better photocatalytic candidate compare to $TiO_2$ because of high life time of photoinduced charge carriers, rapid

electron transfer, crystallization at low temperature and anisotropic growth [20]. In addition ZnO exhibits two fold high electron mobility of 200-300 $cm^2$ $V^{-1}$ $s^{-1}$ than that of $TiO_2$ and facilitated photocharge carrier in photocatalytic reaction [20]. Moreover, the less refractive index of ZnO (2.0) compare to $TiO_2$ (2.5), scarcely scatters light, thereby making it colorless and boosting its transparency [21].

ZnO is a very interesting group II-VI metal oxide with direct band gap of ~ 3.37 eV and large exciton binding energy of 60 meV [22]. Furthermore it absorbs a large portion of UV spectrum and more light quanta, which is highly beneficial to achieve high photocatalytic activity for polluted water treatment [22]. Besides these advantages, ZnO have major challenge in implementing solar light driven photocatalysis reaction as it inevitably obstructing the visible light utilization, which constitutes ~43% of solar energy spectrum. In addition, fast recombination of photoinduced charge carriers, particle aggregation during photocatalytic reaction and photocorrosion are main drawbacks which limits their utilization in large scale [22]. To overcome the aforementioned issues, various strategies have been proposed such as a) surface modification by noble metals [23], b) heterojunction formation with carbonaceous materials [24, 25] and c) coupling with narrow band gap semiconductors [26-30]. Among these approaches, the heterojunction formation through coupling narrow band gap semiconductors has been proved as potential strategy to enhance the lifetime of photoinduced charge carriers by effective charge separation [26]. With narrow band gap semiconductor heterojunctions, the efficient down potential (electrons) and up-potential (holes) transfer from conduction band (CB) and valence band (VB) of ZnO, respectively at interface have proved to enhance the corrosion resistance of ZnO during photocatalytic reactions [7]. For instance, our group recently reported the heterojunction of N-doped ZnO with a narrow band gap semiconductor ($MoS_2$)as efficient photocatalyst for degradation of pharmaceutical pollutant, tetracycline under visible light irradiation [26]. In this heterojunction, $MoS_2$ played dual role by enhancing the photocatalytic activity of ZnO and preventing photocorrosion by managing the photoholes transfer. Kundu et al. [31] demonstrated photocatalytic activity of CdS/ZnO nanorod based heterojunction in dye removal from water under natural sunlight. The CdS heteropartner promote the photocatalytic activity of ZnO nanorods through enhanced visible light absorbance

as well as effective charge separation at hetero-interfaces. It implies that heterojunction based photocatalyst is superior than single photoabsorber.

Graphene has attracted great attention since its discovery in 2004 because of its fascinating physical properties and has been explored intensively for photocatalysis [32, 33]. Being a zero band gap semiconductor, no optical luminescence is observed in graphene. However, band gap can be introduced by downsizing the dimension from 2D to zero dimension. In this lime, graphene quantum dots (GQD) is a new class of graphene derivative with band gap energy due to quantum confinement and edge effects [34]. Recently, GQD have attracted tremendous attention due to excellent photostability, biocompatibility, high specific surface area and abundance of raw materials [35]. GQD have a $sp^2$-hybridized two-dimensional (2D) honeycomb lattice structure with excellent electrons accepting and shuttling properties along with stable photo luminescence [35]. Thus the integration of GQD with wide band gap semiconductors is driving the research to new class of nanoscale functional materials suitable for photocatalytic applications. Recently, Pan et al. [36] have reported nanoscale amine functionalized GQD-$TiO_2$ heterojunction by molecular fusion and hydrothermal method. This heterojunction was exploited for the degradation of methyl orange (MO) dye under visible light irradiation with enhanced photocatalytic performance and photostability. The band gap energy of GQD is tunable and relay on the size and functionalization of its edge sites, which determines the visible light photon harvesting. In addition, the GQD based heterojunctions have been widely investigated as promising catalysts with enhanced charge separation and transfer for photocatalytic applications [37-40].

Some previous reports from our group have focused on nanocomposites of ZnO with narrow band gap materials ($MoS_2$, CdS) and two dimensional (2D) carbonaceous material (reduced graphene oxide) for the removal of organic pollutants from water [22, 26, 32]. In this work, we focus on heterojunction formation using ZnO and GQD, which can be robust and promising catalyst compare to their individual components. Recently, Guo et al. [41] explore the feasibility of GQDs decorated ZnO nanorod based electrode in photoelectrochemcial water splitting. In addition, ZnO-GQD nanocomposites have been widely explored for various applications such as, lithium ion batteries [42], white light emitting diodes [43, 44] and solar

cells [45]. However, to the best of our knowledge, the heterojunction of GQD with ZnO NR has not yet been reported for photocatalytic environmental remediation application. Therefore, in this work we design GQD decorated ZnO nanorods (NR) through hydrothermal method and demonstrate their photocatalytic degradation functionality in color (methylene blue (MB)) and colorless pollutant (carbendazim (CZ)) under sunlight irradiation. In order to explore the role of GQDs, different amount of GQD loading 1 wt%, 2 wt% and 3 wt% in ZnO NR and optimize the best G QDs loading quantity. The ZnO-GQD heterojunction displayed efficient photoinduced charge separation, enhanced light absorption and excellent stability as compared to bare catalysts for removal of the pollutants from water. The strong interfacial interaction between ZnO NR and GQD has been investigated in detail. Therefore, such encouraging results with these heterojunctions can strongly underpin the importance of semiconductor-GQD heterojunctions for promoting photocatalytic activity by directly harvesting solar energy.

## 2. Experimental Section

### 2.1. Materials

For the synthesis of ZnO nanorods, GQD and ZnO-GQD nanocomposites, all the chemicals used were of analytical grade were used as received. Zinc chloride ($ZnCl_2$), sodium hydroxide (NaOH), pyrene ($C_{16}H_{10}$), triethanolamine (TEA), benzoquinone (BQ) which were purchased from Merck, India. Isopropanol (IPA) and nitric acid ($HNO_3$) were obtained by Fisher Scientific. Methylene blue (MB) and carbendazim (CZ) were supplied by Sigma Aldrich. Deionized water (18.2 MΩ-cm) used in synthesis was obtained from double stage water purifier (ELGA PURELAB Option-R7).

### 2.2. Synthesis

#### 2.2.1. Synthesis of ZnO nanorods

ZnO nanorods (NR) were synthesized by hydrothermal method [26]. In a typical experiment, about 2 mL of 15 mL of $ZnCl_2$ solution (0.2 M) in ethanol was added drop wise to 15 mL of NaOH solution (0.5 M) and stirred for 2 h. Later this solution was treated at high temperature (180$^{o}$C) for 12 h in a Teflon-lined stainless steel autoclave, sealed tightly. Finally, the obtained white precipitates were washed thrice with ethanol and water before drying in heating oven at 60$^{o}$C.

### 2.2.2. Synthesis of graphene quantum dots

Graphene quantum dots (GQD) were prepared by using a previously reported synthesis method [36]. In brief, 0.5 g of pyrene were refluxed in $HNO_3$ (40 mL) for 12 h under continuous stirring to form 1,3,6-trinitropyrene. After reaction time, it was allowed to cool down naturally to room temperature and then diluted with 250 mL of deionized water. Subsequently, the solution was filtered to obtained 1,3,6-trinitropyrene as first product. In the second step of reaction, 0.5 g of 1,3,6-trinitropyrene was subjected to ultra-sonication in 0.2 M NaOH solution for its dispersion. Finally the suspension was transferred into Teflon-lined stainless steel autoclave, sealed tightly and maintained at 200°C for 12 h. Once the reaction mixture cooled down naturally to room temperature, the product was filtered through a 0.22 μm microporous membrane to remove insoluble carbon products and further dialyzed in a dialysis bag (retained molecular weight: 3500 Da) for 2 days to remove sodium salt and unfused small molecules. After dialysis, the brownish colored GQD were obtained as final product.

### 2.2.3. Synthesis of ZnO-GQD nanocomposites

The composites were prepared by using hydrothermal synthesis method. In this method, the as prepared ZnO NR was added to the GQD solution in water, with constant stirring for 2 h at room temperature to obtain a homogeneous suspension. After stirring, the suspension was transferred into a Teflon-lined stainless steel autoclave, sealed tightly and maintained at 150°C for 4 h. After that we collected the white precipitate by centrifugation and dried in a vacuum oven at 80°C overnight. By varying the amount of GQD as 1 wt% (0.002 g), 2 wt% (0.004 g) and 3 wt% (0.006 g) in 0.198 g, 0.196 g and 0.194 g of ZnO NR, three heterojunctions were prepared and labelled as ZGQD1, ZGQD2, and ZGQD3, respectively.

### 2.3. Materials characterization

X-ray diffraction (XRD) measurements were performed using Rigaku Smart Lab 9kW rotating anode x-ray diffractometer with Ni-filtered Cu $K_\alpha$ irradiation ($\lambda$ = 0.1542 nm) at 45 kV and 100 mA in 2θ ranging from $10^o$ - $80^o$ with a scan rate of $2^o$ per minute with stepping size of $0.02^o$.

Fourier transform infrared (FTIR) spectra were collected by using Agilent K8002AA Carry 660 instrument. Raman spectroscopic measurements were performed using Horiba LabRAM high resolution UV-VIS-NIR instrument using 633 nm laser. Morphology of the samples was characterized by using field emission scanning electron microscope (SEM), FEI Nova Nano SEM-450 and transmission electron microscope (TEM), FEI Tecnai G2 20 S-twin microscope operating at 200 kV. Energy dispersive x-ray spectra (EDAX) and elemental mapping were obtained by using the same TEM instrument. X-ray photoelectron spectroscopic (XPS) measurements were performed using a high resolution PREVAC photoemission spectrometer having Al $K_\alpha$ (1486.6 eV) dual anode as the source operating at 12 kV anode voltage and 23 mA filament current. The XPS data was collected with pass energy of 50 eV at 6.1 X $10^{-10}$ m bar vacuum using Scienta R3000 electron energy analyzer. As an internal reference for the absolute binding energy, the C-1s peak (284.5 eV) was used. Initially the XPS unit was calibrated using Fermi edge of Ag (KE 1482.544). Optical properties were analyzed by UV-vis diffuse reflectance spectroscopy (DRS) using Perkin Elmer UV/VIS/NIR Lambda 750 spectrophotometer in which polytetrafloroethylene (PTFE) polymer was employed as internal reflectance standard. The Brunauer–Emmett–Teller (BET) surface areas and nitrogen adsorption–desorption isotherms were measured at 77 K on a Quantachrome Autosorb-iQ-MP-XR system. The UV-visible absorption spectra of the samples were recorded using Shimadzu UV-2450 spectrophotometer in the wavelength range 200 to 800 nm. All the photoluminescence (PL) spectra were recorded on Agilent Technologies Cary Eclipse fluorescence spectrometer.

**2.4. Photocatalytic activity**

The photocatalytic activity of bare ZnO, GQD and ZnO-GQD heterojunctions was evaluated by monitoring the decomposition of methylene blue (MB) dye and carbendazim (CZ), a colorless fungicide under natural sunlight irradiation. Briefly, 20 mg of catalyst was suspended in pollutant solution (50 mL, 1 x $10^{-5}$ M). Before illumination, the suspension was continuously stirred for 30 min under darkness to attain the adsorption-desorption equilibrium between pollutants and catalyst. During photocatalysis experiments, 1 mL of photocatalytic suspension

was collected and centrifuged at regular intervals of time and analyzed in UV-visible spectrophotometer. The degradation efficiency can be calculated as:

$$\text{Degradation Rate } (\%) = 1 - \frac{C_t}{C_0}\ X\ 100$$

Here, $C_t$ and $C_o$ represent pollutant concentration at time t and 0, respectively. The intensity of sunlight was measured by a using a LX-101A digital luxmeter.

## 3. Results and Discussion

### 3.1. Synthesis and structural studies

The ZnO nanorods decorated with GQD in varying compositions and the control samples were synthesized by a facile hydrothermal route using appropriate precursors. In this work, GQD amount in ZnO NR was varied from 1 wt% to 3 wt% to prepare the semiconductor heterojunctions. To decipher the crystal structure and heterojunction formation between ZnO and GQD, x-ray diffraction (XRD) measurements were performed and presented in Figure 1. XRD patterns of ZnO in Figure 1(a) shows the presence of characteristic diffraction peaks, which are positioned at 2θ values of 31.5$^o$, 34.4$^o$, 36.3$^o$, 47.3$^o$, 56.4$^o$, 62.9$^o$, 66.3$^o$, 67.9$^o$ and 69.1$^o$ and could be indexed to (100), (002), (101), (102), (110), (103), (200), (112) and (201) lattice planes of hexagonal Wurtzite structure, respectively (JCPDS no. 36-1451) [26]. Figure 1 (b) presents the XRD pattern obtained for GQD exhibit broad peak, which is centered on 2θ value around 24$^o$ and could be attributed to (002) lattice plane of carbon skeleton with hexagonal phase (JCPDS no. 75-1621), while the presence of a small diffraction peak around 30$^o$ signifies the few layered GQD [46]. The broad diffraction peak of GQD reveals the low crystallinity and small size. The ZnO-GQD heterojunction retained all characteristic diffraction peaks of ZnO with weakened diffraction intensity with increasing GQD amount. This decrease in intensity and appearance of no diffraction peak due to GQD could be attributed to the weak diffraction intensity and low amount of GQD in heterojunction as previously reported in literature [37].

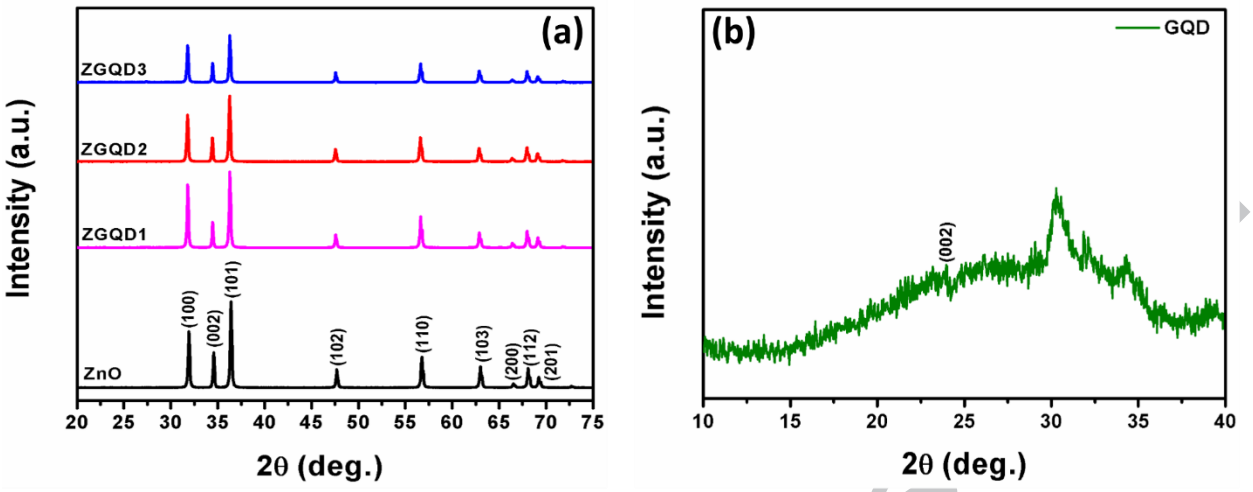


**Figure 1.** (a) XRD patterns of ZnO, ZGQD1, ZGQD2 and ZGQD3 heterojunctions; (b) XRD pattern of GQD.

Figure 2(a) shows the FTIR spectra of GQD, ZnO, ZGQD1, ZGQD2 and ZGQD3 heterojunctions, which reveal the presence of C=O (1727 $cm^{-1}$), C=C (1630 $cm^{-1}$), COOH (1382 $cm^{-1}$) and C-O (1020 $cm^{-1}$) functional groups in GQD, which are consistent with literature [47]. The peak at 1505 $cm^{-1}$ corresponds to the N-H vibration, while broad band in 3500-3000 $cm^{-1}$ range could be attributed to the O-H stretching vibrations of adsorbed water molecules in GQD [36]. FTIR spectra of ZnO NR (Figure 2e) exhibit the peaks at 925 $cm^{-1}$ and 658 $cm^{-1}$ corresponding to Zn-O stretching vibrations [22], while the peaks due to their bending vibrations can be seen in the 500-400 $cm^{-1}$ range. It can be seen clearly that, characteristic vibrational peaks of GQD and ZnO are present in all three heterojunctions confirming the successful formation of ZnO-GQD hybrid.

Raman spectroscopy was used to obtain additional structural information on ZnO NR, GQD and the ZGQD heterojunctions. Raman spectra of control samples and heterojunctions have been presented in Figure 2(b). Pure ZnO exhibit the characteristic Raman peaks at 332 $cm^{-1}$, 375 $cm^{-1}$ and 435 $cm^{-1}$, which correspond to $A_1$, $E_2$ and $A_1$ (TO) vibrational modes of hexagonal structure, respectively. GQD shows presence of two Raman peaks at 1353 $cm^{-1}$ and 1586 $cm^{-1}$ which can be assigned as D-band (disordered $sp^2$ carbon) and G-band (ordered graphite), respectively. The intensity ratio of D-band to G-band ($I_D/I_G$ = 1.01) is a measure of disorder in its lattice structure associated with grain boundaries, vacancies and amorphous carbon. It is noteworthy to mention that the vibrational modes of ZnO can also be seen in ZGQD1, ZGQD2,

and ZGQD3 heterojunctions along with two additional Raman bands which corresponds to GQD confirming the presence of both the components.

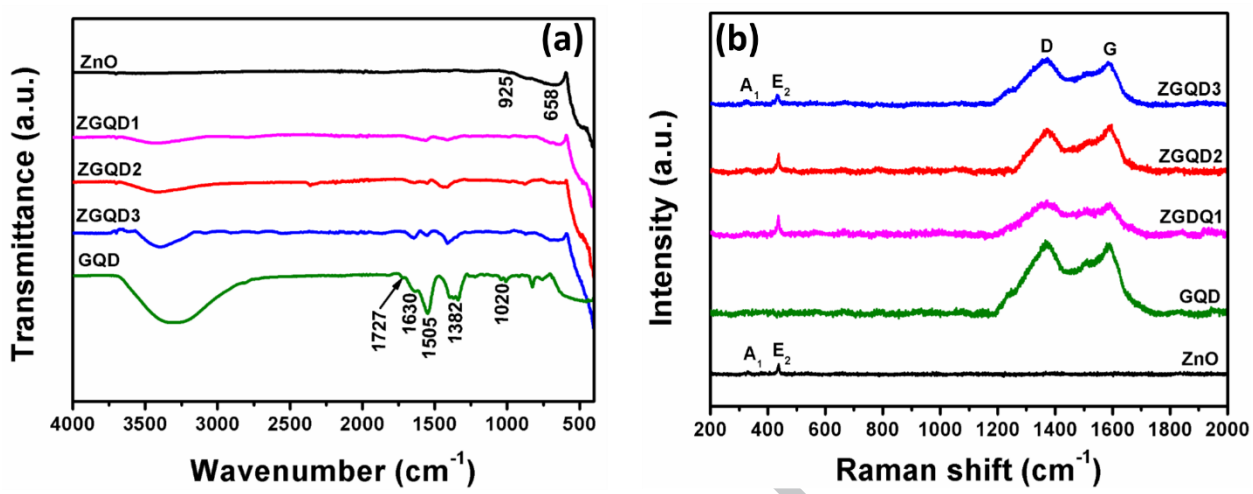


**Figure 2.** (a) FTIR spectra and (b) Raman spectra of ZnO, GQD, ZGQD1, ZGQD2 and ZGQD3 heterojunctions..

### 3.2. Morphological and compositional studies

The morphological studies of all photocatalysts were carried out by scanning electron microscopy (SEM) and transmission electron microscopy (TEM) analysis. SEM micrographs have been presented in Figure S1, which reveals the rod-like morphology, uniform distribution and ~ 1 µm length of ZnO NR (Figure S1 (a)). Same morphology of NR was retained after heterojunction formation with GQD as presented in SEM images of ZGQD1, ZGQD2, and ZGQD3 heterojunctions (Figure S1 b, c, d). More detailed insights on the morphology of bare catalysts and heterojunctions have been revealed by TEM measurements presented in Figure 3. From Figure 3, the uniform distribution of GQD implies that GQD are in homogenous in particle size which is less than 5 nm (Figure 3a, 3b, 3c). While, ZnO shows rod like morphology complementing the SEM results (Figure 3d). Interestingly, in the heterojunctions the GQD can be clearly visible on the surface of ZnO NR to form intimate contact between them, which can facilitate charge transfer across heterojunctions (Figure 3e). In addition to this, HRTEM images of ZGQD2 (representative sample) has also been provided in Figure 3(f) and Figure S2 (refer supporting information) to confirm the successful decoration of GQD on ZnO NR. Lattice fringes

with d-spacing of 0.21 nm corresponding to (002) crystal plane of GQD could be evidenced from the high magnification images. Furthermore, the lattice fringes with d-spacing of 0.26 nm can be assigned to the (002) plane of hexagonal ZnO. The intimate contact between lattice fringes of GQD and ZnO confirms the heterojunction formation. The elemental mapping of ZGQD2 shown in Figure 3(g) confirms the coexistence of all elements of the heterojunction. Energy dispersive x-ray spectroscopy (EDAX) measurements of ZnO and ZGQD2 heterojunction were recorded to confirm the presence of constituent elements (Zn, O, C in ZGQD2 and Zn, O in ZnO) as can been seen in Figure S3 (refer supporting information).

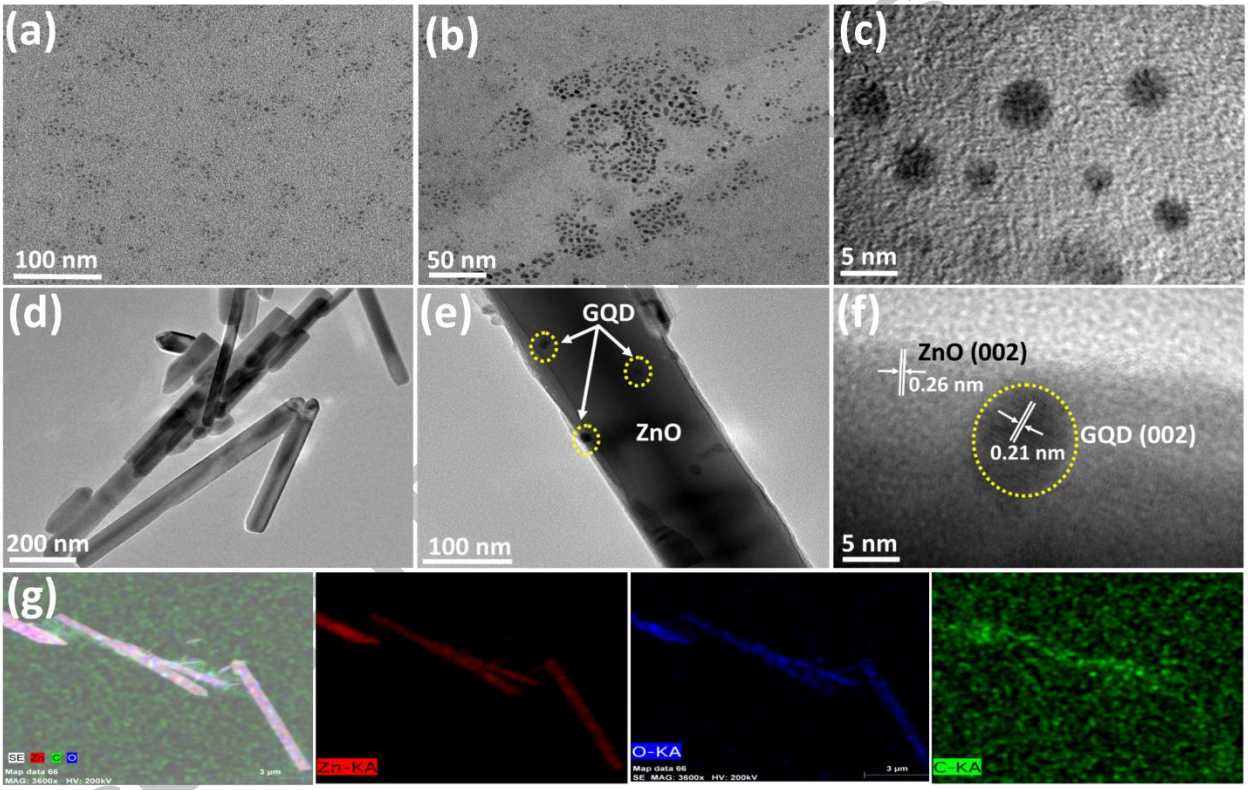


**Figure 3.** TEM images of (a, b, c) GQD; (d) ZnO NR; (e, f) TEM and HRTEM images of ZGQD2; (g) elemental mapping showing the presence of Zn, O and C in ZGQD2 heterojunction.

The surface composition and chemical states of constituent elements of ZGQD2 heterojunction as representative photocatalyst has been investigated by using x-ray photoelectron spectroscopy (XPS) in the binding energy range of 0-1400 eV. Figure 4(a) presents the survey spectrum of ZGQD2 heterojunction, the presence of Zn-2p, O-1s and C-1s peaks can be observed in full spectra. Figure 4(b) shows the C-1s spectra of ZGQD2 with four

binding energy peaks. First binding energy peak at 284.4 eV could be assigned to the C-C bonds in graphitic structure of GQD. While binding energy peaks at 286.4 eV, 287.8 eV, and 288.9 eV corresponds to the oxygen containing functional groups such as C–O (epoxy and alkoxy), C=O (carbonyl), and –COOH (carboxylic) groups, respectively. Therefore, the C-1s spectrum of ZGQD2 confirms the heterojunction formation between ZnO and GQD. The high resolution XPS spectra of Zn-2p of ZnO NR and ZGQD2 are shown in Figure 4(c) and 4(d), respectively. The ZnO NR exhibit two binding energy peaks at 1021.6 eV (Zn-$2p_{3/2}$) and 1044.4 eV (Zn-$2p_{1/2}$), which correspond to the $Zn^{2+}$ state. It is noteworthy to mention here that, Zn-2p of ZGQD2 heterojunction shows binding energy peaks at 1021.3 eV (Zn-$2p_{3/2}$) and 1044.5 eV (Zn-$2p_{1/2}$). This slight shift of Zn-2p binding energy peaks could be attributed to the strong interfacial interactions between ZnO and GQD. Figure 4(e) and 4(f) show the high resolution O-1s spectra of ZnO NR and AGQD2, respectively. The ZnO NR exhibit two binding energy peaks at 530.2 eV and 531.9 eV, which signify non-stoichiometric oxygen atoms and the lattice oxygen contribution from ZnO, respectively. While the binding energy peaks of O-1s of ZGQD2 heterojunction appears at slightly higher binding energy (531.2 eV and 532.9 eV), which could be attributed to the electronic interactions in heterojunction as previously reported [1]. The above XPS results further confirmed the successful combination of ZnO and GQD to form highly efficient heterojunction which anticipated to enhance charge transfer across hetero-interface, which will support to increase the photocatalytic activity.

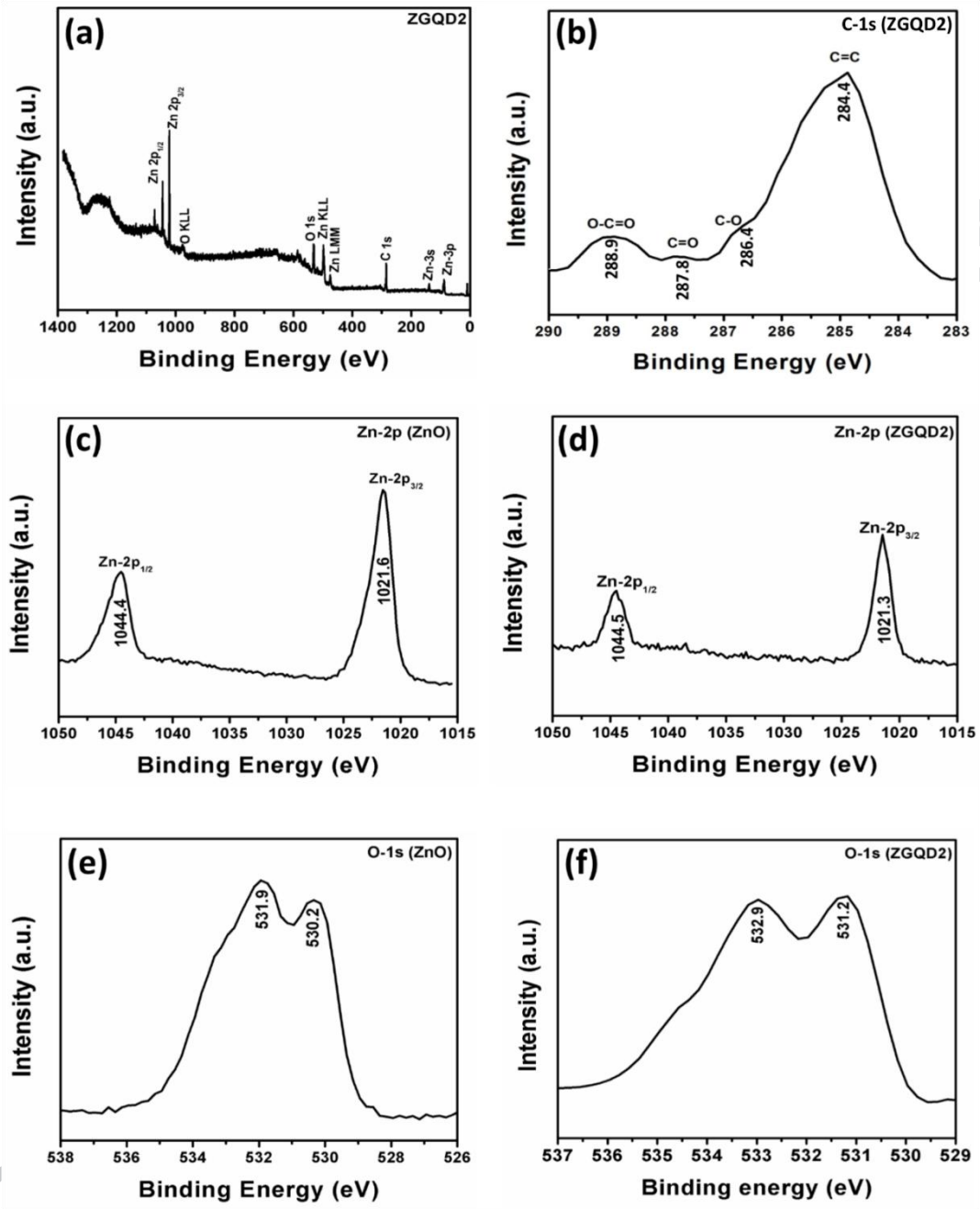


**Figure 4.** XPS spectra: (a) survey spectrum of ZGQD2 heterojunction, (b) C-1s (ZGQD2), (c) Zn-2p (ZnO), (d) Zn-2p (ZGQD2), (e) O1s (ZnO) and (f) O1s (ZGQD2).

### 3.3. Physical properties studies

The optical properties of ZnO-GQD heterojunctions and bare catalysts were evaluated by UV-visible diffuse reflectance spectroscopy (DRS). Figure 5(a) depicts the UV-visible absorption

spectra of ZnO, ZGQD1, ZGQD2, and ZGQD3 heterojunctions with different amount of GQD on ZnO NR. It is clear that ZnO shows distinct absorption in UV region and exhibit absorption edge around 386 nm due to electrons promotion from VB to CB and no absorption in visible region (λ > 400 nm) was observed. The corresponding band gap energy obtained for this absorption wavelength is 3.21 eV which is in good agreement with literature reports [22, 26]. Red shift in the absorption edge from 386 nm to 392 nm, 398 nm and 402 nm, with increasing absorption intensity, can be seen clearly as the amount of GQD increases to 1 wt%, 2 wt% and 3 wt%, respectively in ZnO-GQD heterojunctions. This implies the increased visible light absorption in 400-800 nm range upon GQD loading. Similar observations to enhance the visible light absorption on $TiO_2$-GQD nanocomposites have been recently reported by Min et al. [37] . Figure S4 (refer supporting information) shows the band gap values of the heterojunctions obtained from Kubelka-Munk plot and found to be 3.16 eV (ZGQD1) , 3.11 eV (ZGQD2) and 3.08 eV (ZGQD3) which were lower than bare ZnO NR (3.21 eV). Therefore, it is inferred that the heterojunction formation between ZnO and GQD extends the absorption towards visible region which expected to improve the visible light activity when illuminated under natural sunlight.

Surface area of nanomaterials is critical for their functional properties and applications such as photocatalysis related to their contact interfaces. To investigate the specific surface area, Brunauer-Emmett-Teller (BET) ($S_{BET}$) gas physisorption measurements were performed. The nitrogen adsorption-desorption isotherm of ZGQD2 heterojunctions (representative photocatalyst) at 77 K obtained using multipoint BET method is presented in Figure 5(b). The isotherm present a characteristic type IV curve with a pronounced hysteresis loop. The ZGQD2 heterojunction exhibits high surface area, which was estimated to be 353.447 $m^2 g^{-1}$. Such high value of specific surface area has been well reported in literature for GQD based nanocomposites [48]. This large surface area of heterojunction is highly desirable to provide more interfacial contact region between the two components for photoinduced charge transport and abundant exposed edge sites to adsorb more pollutants.

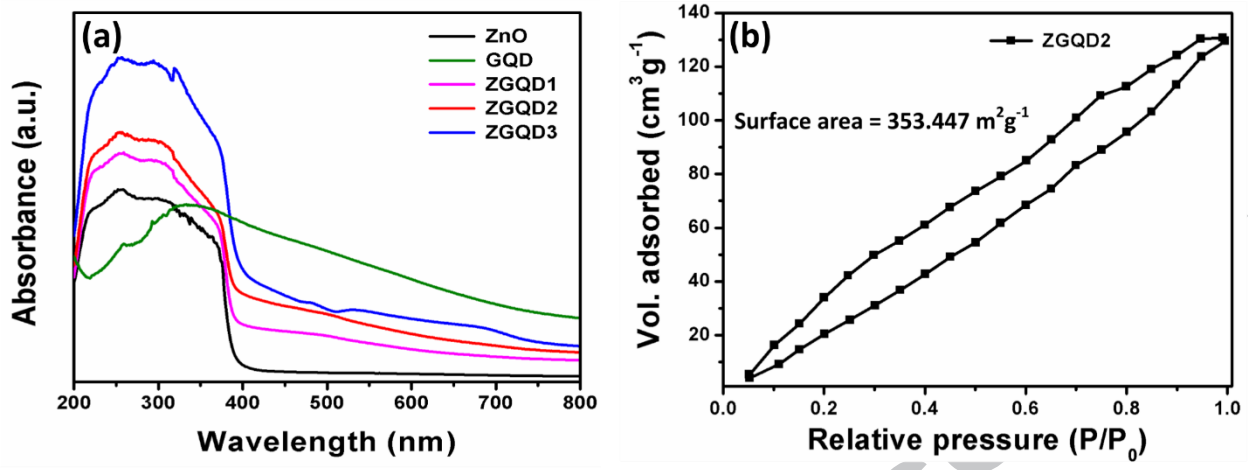


**Figure 5.** (a) UV-visible diffuse reflectance spectra of ZnO, ZGQD1, ZGQD2 and ZGQD3 heterojunctions, (b) $N_2$ adsorption-desorption isotherms of ZGQD2 heterojunction.

### 3.4. Photocatalytic activity studies

The photocatalytic performance of all the prepared catalysts were studied by evaluating the degradation of MB (colored pollutant dye) and CZ (colorless hazardous fungicide) under natural sunlight irradiation having an intensity of 9.2 X $10^4$ lux. The successive time dependent UV-vis absorption spectra of degradation of MB are presented in Figure 6. Prior to the sunlight irradiation, the incubation period of 30 min in dark condition lead to the adsorption-desorption equilibrium between the dye molecules and the catalysts. The photocatalysts reached their saturated adsorption as presented in Figure S5 (refer supporting information), which reveals nearly same adsorption of pollutant over catalyst surface in 30 min and 60 min. The major absorption peak of MB at 663 nm diminishes gradually indicating the decomposition of MB dye under sunlight irradiation in the presence of catalysts. The photolysis degradation of MB (without photocatalyst) was also tested for the identical duration (70 min) and negligible degradation was observed (Figure 6a). For more understanding of photocatalytic degradation experiments of MB with bare ZnO and GQD were also carried out under sunlight irradiation. The experimental results presented in Figure 6(b, c) shows that in presence of ZnO and GQD catalysts, the concentration of MB decreases meagerly even after 70 min of illumination. While, the successive time dependent UV-vis spectra of MB degradation over ZGQD1, ZGQD2 and ZGQD3 heterojunctions, presented in Figure 6 d, 6e, and 6f show significant degradation of MB

in 70 min of sunlight irradiation. The improved photocatalytic activity of ZnO-GQD heterojunctions is ascribed to the better dye pollutant adsorption as well as photosensitization effect of ZnO by GQD. The later effect enable the catalyst to utilize the maximum fraction of visible light from sunlight as previously reported in literature [41, 49, 50] . As a result ZGQD2 heterojunction, showed high photocatalytic degradation rate than bare ZnO and GQD. It is clearly advocate that GQD loading over ZnO NR significantly enhances the photocatalytic activity of the heterojunctions due to improved charge separation across ZnO-GQD interface and their fast transfer to reaction sites over catalyst surface. Overall comparison, the highest photocatalytic activity was achieved with ZGQD2 heterojunction, it reveals that the optimum loading of GQD is 2 wt%. Because under the optimized GQD loading results in fine interfacial contact for efficient charge transfer, homogenous dispersion and abundant reaction sites to degrade the dye pollutant. However in the case of high loading of GQD (more than 2 wt%) decreases the photocatalytic rate, which might be attributed to the following factors: (i) higher amount of GQD is prone to the self-aggregation weakening the heterojunction contact interface and decreases the photocatalytic activity and (ii) poor light adsorption by the heterojunction resulting in lesser photoinduced charge generation, which hamper the photocatalytic activity. This justifies the best photocatalytic activity of the optimized heterojunction, ZGQD2 and decreased activity with heterojunction having 3 wt% of GQD. The kinetic curves of the MB degradation over all catalysts under sunlight irradiation have been presented in Figure 7(a, b), which shows the degradation follows pseudo first order kinetics as per following equation:

$$\ln (C/C_0) = -kt$$

Here, $C_0$ and C are MB concentration at time 0 and t, respectively and k is rate constant ($min^{-1}$) of reaction. Furthermore, the histogram in Figure 7(c) presents comparative photocatalytic degradation rate (%) of all catalysts, which follows the order as ZGQD2 (95%) > ZGQD3 (92%) > ZGQD1 (88%) > ZnO (28%) > GQD (8%). Hence, the corresponding rate constant (k) values for MB degradation with GQD and ZnO were 0.0011 $min^{-1}$ and 0.0051 $min^{-1}$. While, rate constant calculated for ZGQD1, ZGQD2 and ZGQD3 were 0.0302 $min^{-1}$, 0.0439 $min^{-1}$ and 0.0376 $min^{-1}$, respectively revealing enhanced photocatalytic performance of heterojunctions as compared to bare catalysts (Figure 7d). The rate constant of ZGQD2 is superior (8 folds) than bare ZnO. These

experimental findings demonstrate the synergistic effect of optimal loading of GQD on to ZnO and the heterojunction formation boosts the photocatalytic activity in removal of organic pollutant from water.

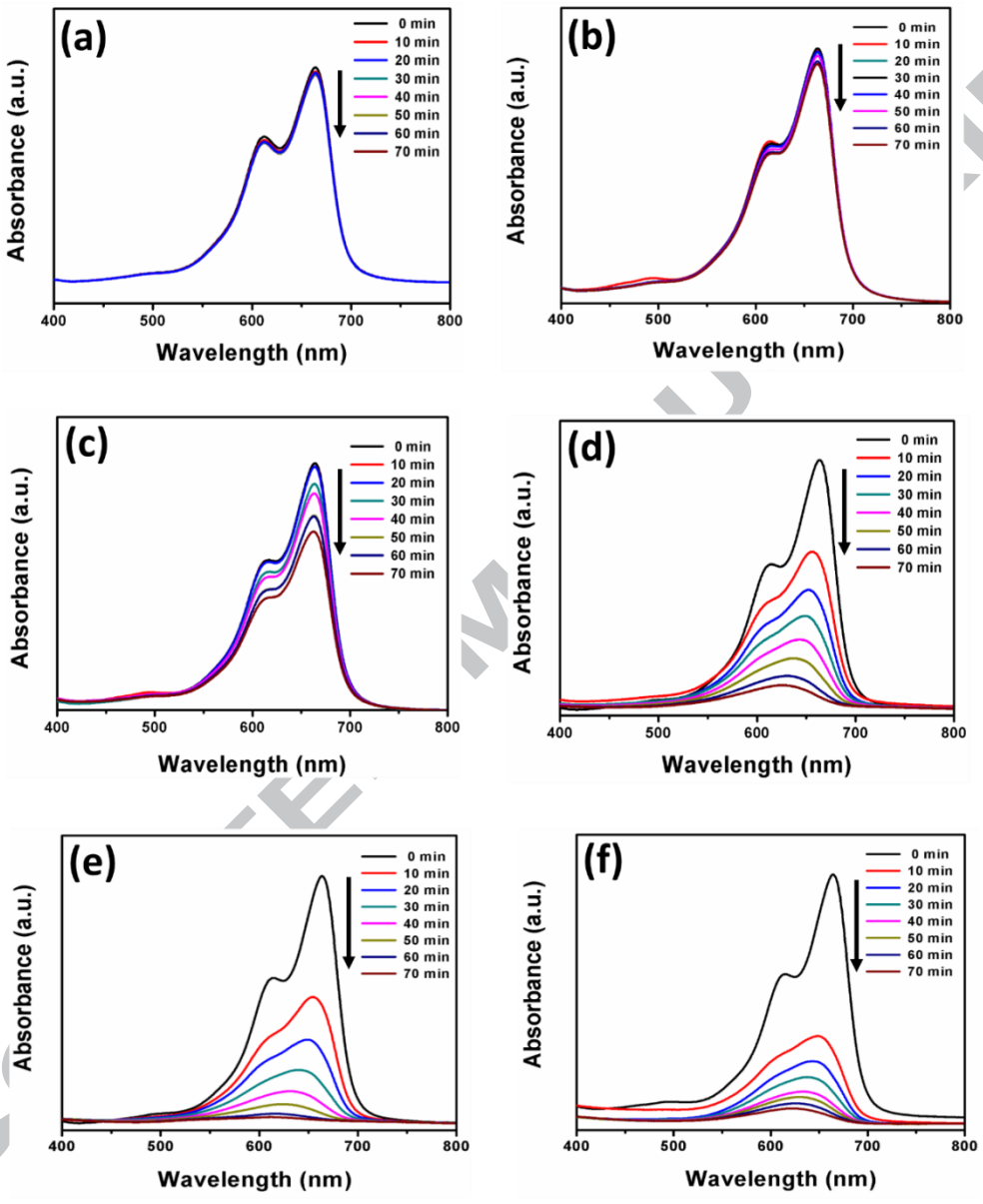


**Figure 6.** Successive time dependent UV-vis absorption spectra of MB dye (1 x $10^{-5}$ M) degradation: (a) without catalyst, (b) in presence of GQD, (c) ZnO, (d) ZGQD1, (e) ZGQD2, and (f) ZGQD3 under natural sunlight irradiation.

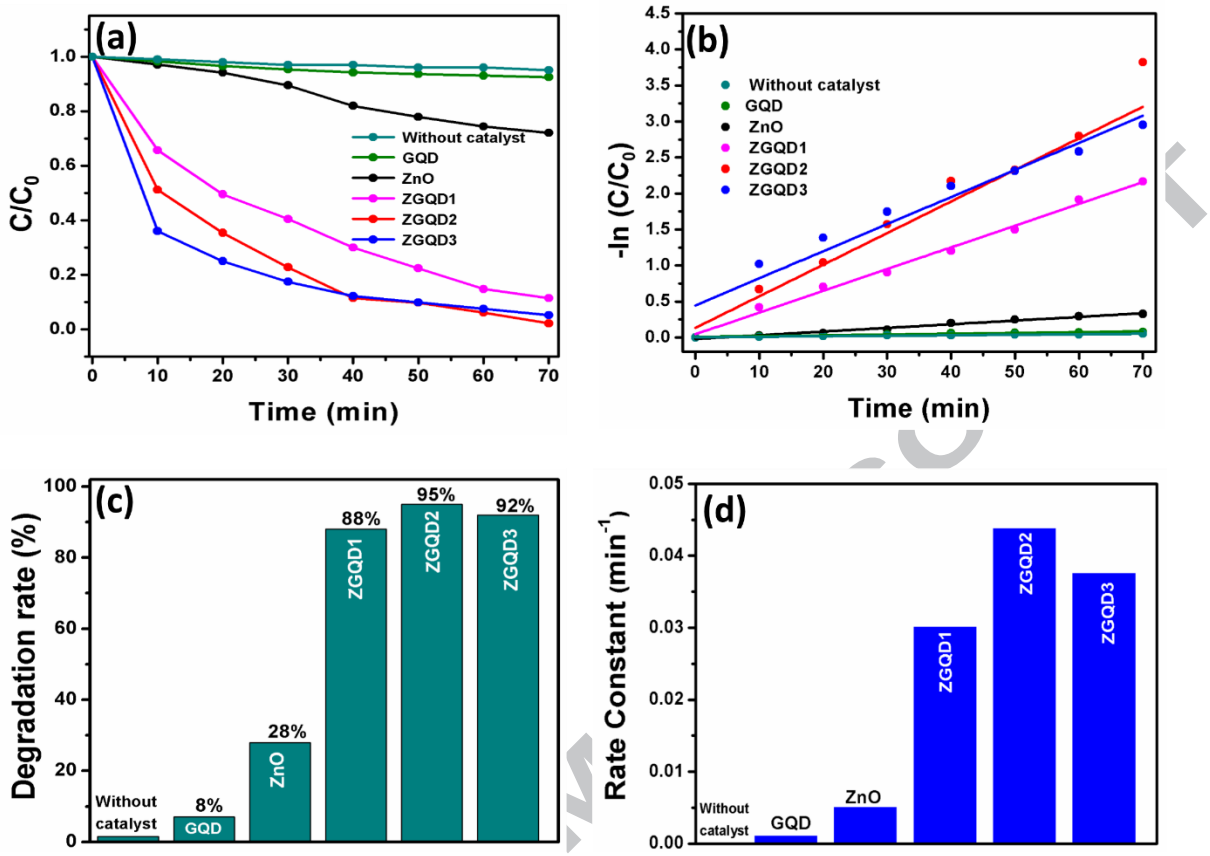


**Figure 7.** (a) Kinetic curves for degradation of MB, (b) -ln($C/C_0$) vs. time curve for degradation of MB, (c) histogram showing comparative degradation rate (%) of MB with the photocatalysts under natural sunlight irradiation and (d) bar graph showing the values of the rate constants for all the photocatalysts.

In order to ensure the degradation of dye pollutant is solely due to photocatalytic nature of the heterojunctions and not contributed from photosensitization of the MB dye, we demonstrate similar photocatalytic dye degradation experiments using colorless pollutant CZ. CZ is a benzimidazole fungicide, which is very stable under natural environmental conditions and detected in surface waters. It has been identified as one of the most hazardous pollutants as its exposure is highly toxic to human beings and aquatic life [22]. Therefore, the elimination of CZ from water by a facile process is of great significance. The photocatalytic degradation of CZ was studied by monitoring its main absorbance peak at 285 nm and corresponding time dependent UV-visible spectra have been presented in Figure 8. Figure 8(a, b and c) presents the UV-vis spectra of photocatalytic degradation of CZ without catalyst, bare GQD and ZnO,

respectively. While the diminishing of main absorbance peak of CZ in presence of ZGQD1, ZGQD2 and ZGQD3 heterojunctions can be seen in Figure 8 (d, e and f). Kinetic plots for CZ degradation over various catalysts have been presented in Figure 9 (a, b) revealing the pseudo first order kinetics of the degradation reaction. The calculated degradation rate (%) of was GQD (13%), ZnO (40%), ZGQD1 (76%), ZGQD2 (94%) and ZGQD3 (91%) as displayed in Figure 9 (c). While, the corresponding rate constants for CZ degradation was 0.0032 $min^{-1}$, 0.0076 $min^{-1}$, 0.0198 $min^{-1}$ , 0.0362 $min^{-1}$ and 0.0356 $min^{-1}$ over GQD, ZnO, ZGQD1, ZGQD2 and ZGQD3, respectively (Figure 9d) showing the superior photocatalytic activity of ZGQD2 heterojunction in this case as well. All these experimental results demonstrate the ZnO-GQD heterojunctions as efficient catalysts for removal of variety of pollutants from water using sunlight irradiation.

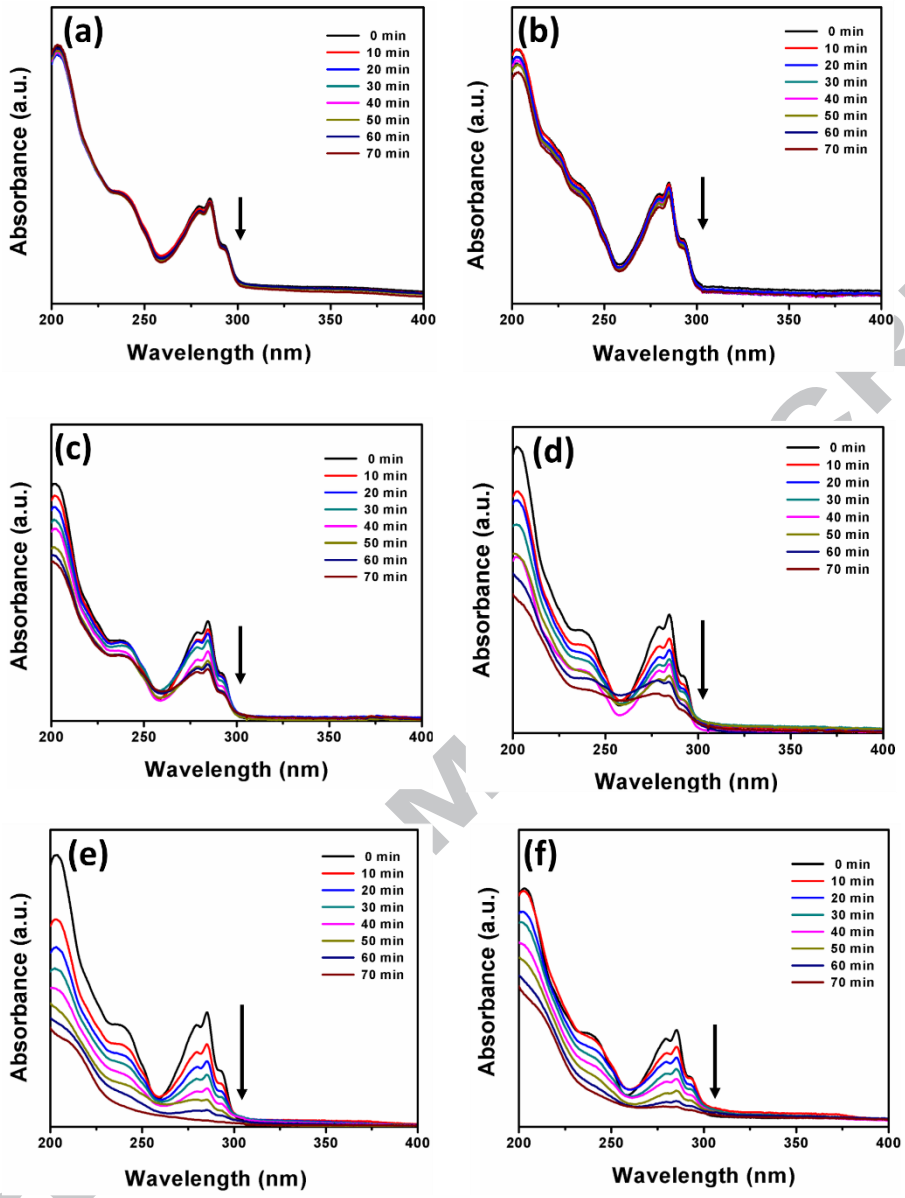


**Figure 8.** Successive time dependent UV-vis absorption spectra of CZ solutions (1 x $10^{-5}$ M) degradation (a) without catalyst, (b) in presence of GQD, (c) ZnO, (d) ZnO-GQD1, (e) ZnO-GQD2, and (f) ZnO-GQD3 under natural sunlight irradiation.

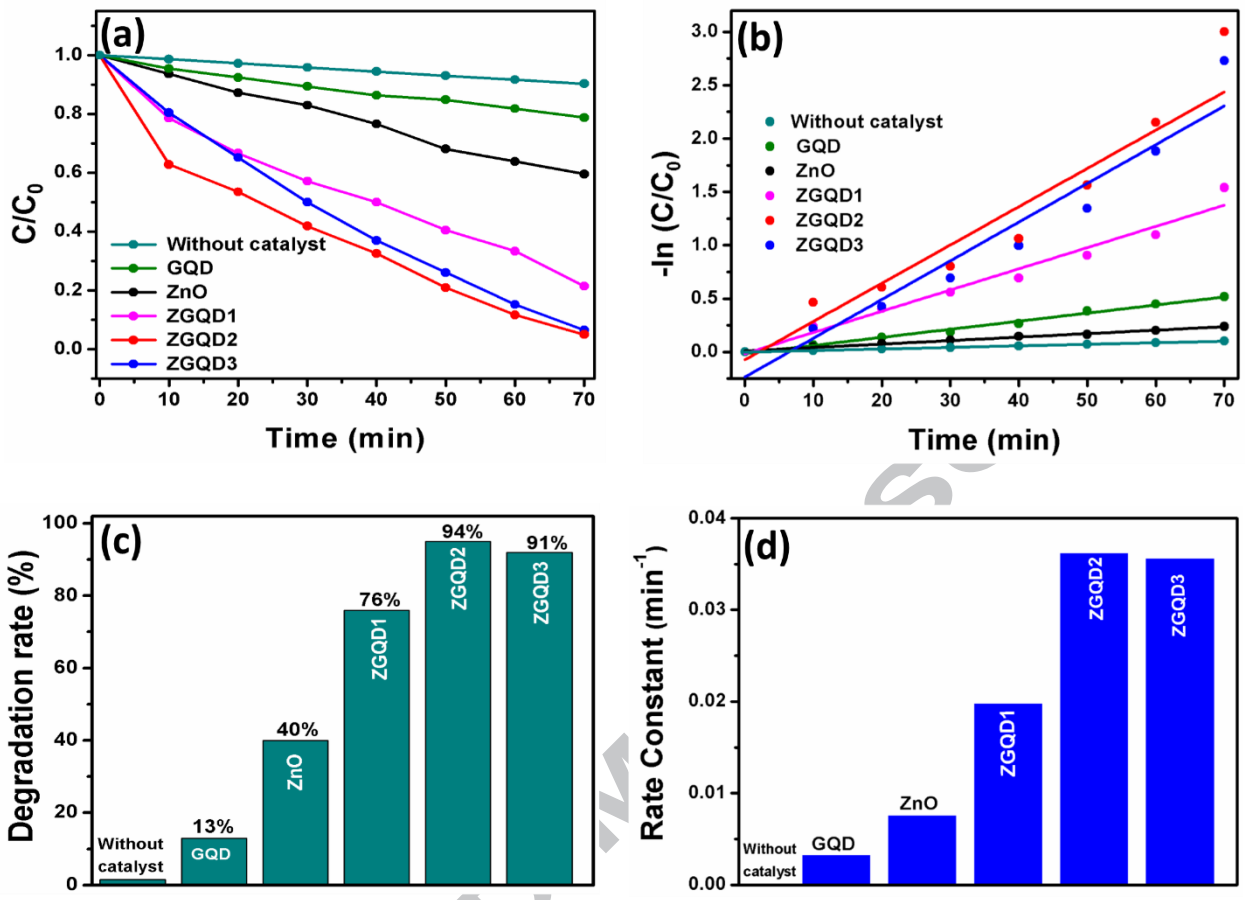


**Figure 9.** (a) Kinetic curves for degradation of CZ, (b) -ln($C/C_0$) vs. time curve for degradation of CZ, (c) histogram showing comparative degradation rate (%) of CZ with the photocatalysts under natural sunlight irradiation and (d) bar graph showing the values of the rate constants for all the photocatalysts.

### 3.5. Photoluminescence studies

The recombination of photoinduced charge carriers decreases the activity of the photocatalyst. Therefore, to study the effect of GQD loading on recombination probability of photoinduced charge carriers, the photoluminescence (PL) spectra was recorded for all prepared photocatalysts and presented in Figure 10. Figure 10 (a) presents UV-vis spectra of ZnO NR with strong absorption band at 372 nm, which was taken as excitation wavelength to record the PL spectra at room temperature. The higher PL emission intensity indicate the high recombination rate of photoinduced charge carriers [1]. It can be seen clearly from Figure 10 (b) that ZnO NR exhibit PL emission peaks at 440 nm and 490 nm and 510 nm. These PL emission

bands originated from recombination of photoinduced charge carriers, zinc interstitial defects and oxygen vacancies in pure ZnO, as previously reported [1, 26]. The violet emission band at 440 nm could be attributed to the zinc interstitial defects, while blue emission band at λ=490 nm and the green emission band at λ=510 nm could be attributed to surface states and oxygen vacancies in the ZnO NR [1, 51]. Interestingly, the emission intensity of ZGQD1, ZGQD2 and ZGQD3 heterojunctions decreases as compared to bare ZnO, which indicate the decreased recombination of photoinduced electron-hole pairs, which is highly beneficial for photocatalytic activity. Very importantly, the ZGQD2 heterojunction exhibits notably decreased PL emission intensity among all the photocatalysts. It infers that the effective separation of photoinduced charge carriers at heterojunction sample could prolongs minority carrier lifetime and thus boost interfacial transfer for enhanced photocatalytic activity under sunlight. It is noteworthy to mention that, the GQD shows absorption in UV-vis region and fluorescent properties. The characteristic absorption band of GQD in UV range corresponds to the $\pi \rightarrow \pi^*$ transition of C=C of graphene structure (Figure S6a in supporting information) [52] . When excitation wavelength was 340 nm, then GQD exhibit green fluorescence with PL emission band in 500-600 nm (Figure S6b in supporting information). The inset in Figure S6 (a) shows photographs of GQD aqueous solution under white light and under UV light (365 nm) with green fluorescence. The PL emission of GQD depends on excitation wavelength and can be correlated with size polydispersion of quantum dots [52]. It is worth to mention here that, GQD do not exhibit any absorption band in infrared region (refer Figure S6 in supporting information).

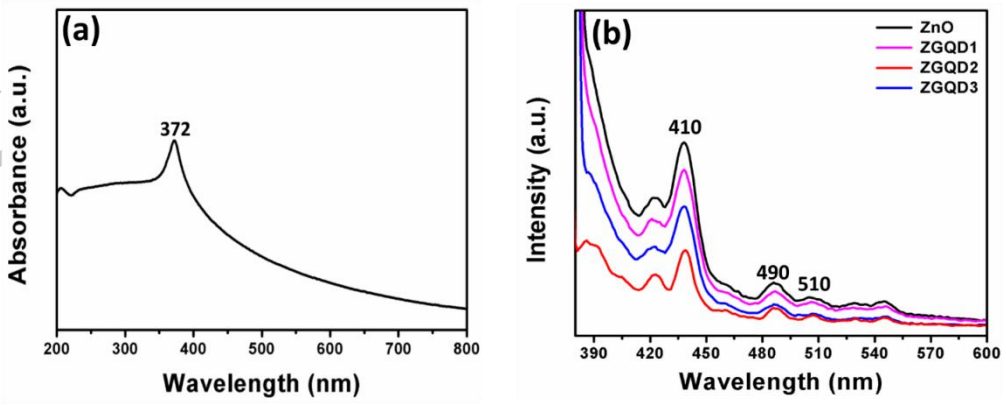


**Figure 10.** (a) UV-vis absorption spectrum of ZnO NR, (b) photoluminescence spectra of ZnO, ZGQD1, ZGQD2 and ZGQD3 heterojunctions.

### 3.6. Mechanism of photocatalytic activity

The active species trapping during photocatalytic degradation of MB with ZGQD2 heterojunction has been investigated by adding different scavengers and corresponding results can be seen in Figure 11. In this regard, triethaonlamine (TEA) was used as hole ($h^+$) scavenger, isopropanol (IPA) as hydroxyl radical ($^*OH$) scavenger and benzoquinone (BQ) as superoxide ion radical ($O_2^{-*}$). As it can be seen from Figure 11 that the photocatalytic degradation of MB has decreases to 26% by addition of TEA advocate the key role played by $h^+$ in degradation. However, the photocatalytic degradation rate has drops to 48% with IPA as scavenger, which reveals the active role of $^*OH$ for pollutants removal under natural sunlight irradiation. On contrary, the photocatalytic degradation was slightly influenced by the presence of BQ indicating that $O_2^{-*}$ are not generated during photocatalytic reaction.

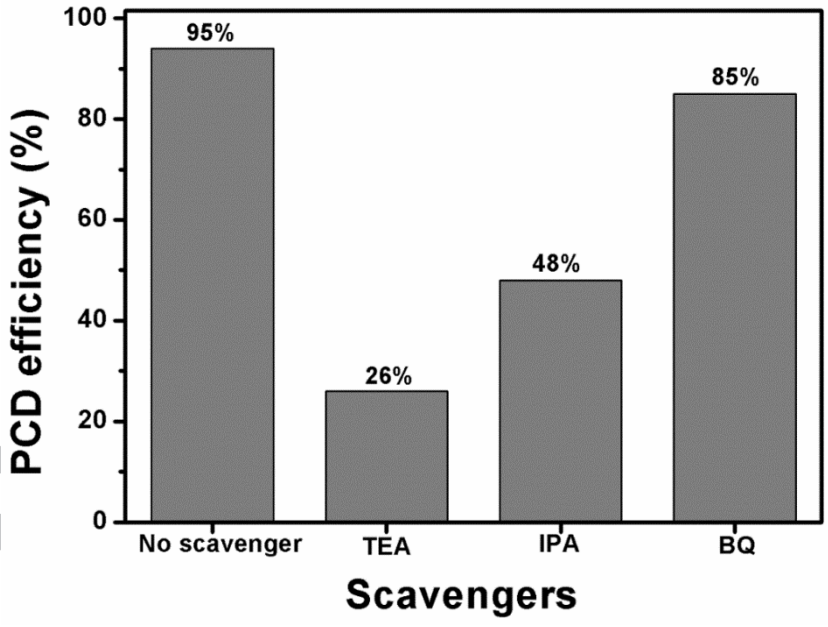


**Figure 11.** Effects of scavengers on photocatalytic degradation efficiency (PCD) of MB by using ZGQD2 heterojunction under natural sunlight irradiation.

Based on the above results, the underlying mechanism of photocatalytic degradation of pollutant (MB/CZ) over ZnO-GQD heterojunctions under sunlight irradiation is proposed in Scheme 1. It has been previously reported in the literature that GQD acts as photosensitizers to semiconductors and are responsible for the enhanced absorption in visible region, which

eventually increases the photocatalytic performance by generation of more photoinduced charge carriers [37, 50]. Some of the previous studies have reported the conduction band (CB) position of GQD around -3.0 to -3.5 eV vs vacuum energy level, which is more negative than CB position of ZnO (-4.19 eV vs vacuum energy level) [36, 50]. The position of CB and valence band (VB) of ZnO NR can be calculated by applying following equations reported in literature,

$$E_{CB} = X - E_e - 1/2E_g$$

$$E_{CB} = E_{VB} - E_g$$

Here, $E_{CB}$ and $E_{VB}$ are the conduction band and valence band edge potentials, $X$ is the electronegativity of the semiconductor (ZnO is 5.79 eV [53], $E_e$ is the energy of free electrons on the hydrogen scale (4.5 eV); and $E_g$ is the band gap energy of the semiconductor (ZnO is 3.21 eV, as calculated form DRS data). By applying the above mentioned equation, $E_{CB}$ and $E_{VB}$ obtained for ZnO was determined to be -0.31 eV and 2.89 eV, respectively which correspond to the -4.19 eV and 7.39 eV vs vacuum energy level. When photocatalytic reaction mixture was subjected to sunlight, the photoexcitation of both ZnO (by UV photons) and GQD (by visible light photons) takes place, which leads to electron-hole pairs' formation. The strong interfacial contact between ZnO and GQD leads to the photoexcited electrons transfer from more negative CB of GQD to less negative CB of ZnO. Meanwhile, the photoinduced holes move up-potential from VB of ZnO to VB of GQD, which triggers the photoinduced electron-hole separation efficiently across the heterojunction [37]. The transferred electrons from CB of ZnO cannot produce $O_2^{-*}$ from dissolved oxygen due to more positive CB potential of ZnO (-0.31 eV vs NHE) as compared to the reduction potential of -0.33 eV vs NHE ($O_2$/ $O_2^{-*}$) [26]. However, these electrons can produce $H_2O_2$ by reacting with $O_2$ and $H^+$ ions due to more positive reduction potential of $O_2/H_2O_2$ (0.695 eV vs NHE). Furthermore, the highly oxidizing species, $^*$OH radicals were produced by degradation of $H_2O_2$ molecules in the presence of light energy and photoinduced electrons [22, 26]. These $^*$OH radicals results in the mineralization of pollutants (MB/CZ) into $CO_2$ and $H_2O$. In contrast, the photoinduced $h^+$ from VB of GQD also degraded pollutants directly as they cannot produce $^*$OH from $OH^-$ and $H_2O$ due to more positive reduction potential of $OH^-/^*OH$ (2.38 eV vs NHE) and $H_2O/^*OH$. The entire photocatalytic reaction mechanism can be proposed as follows:

$$ZnO\text{-}GQD + h\nu\ (sunlight) \rightarrow ZnO\text{-}GQD\ (h^+\ VB + e^-\ CB)$$

$$GQD\ (e^-\ CB) \rightarrow ZnO\ (e^-\ CB)$$

$$ZnO\ (h^+\ VB) \rightarrow GQD\ (h^+\ VB)$$

$$ZnO\ (e^-\ CB) + H^+ + O_2 \rightarrow H_2O_2$$

$$H_2O_2 + e^- + h\nu \rightarrow {}^*OH + OH^-$$

$${}^*OH + h^+ + pollutants \rightarrow Degradation\ products$$

Therefore, it can be inferred that the formation of $^*OH$ and $h^+$ as active species over photocatalyst surface oxidizes the organic pollutants and results in enhanced photocatalytic performance. Moreover, better solar spectrum utilization from UV to visible region, fast charge transfer across heterojunction and high specific surface area of GQD contributes towards high photocatalytic activity by harvesting solar energy. Furthermore, Table 1 shows the superior photocatalytic activity of our ZnO-GQD heterojunction as compared to similar materials based on ZnO and GQD.

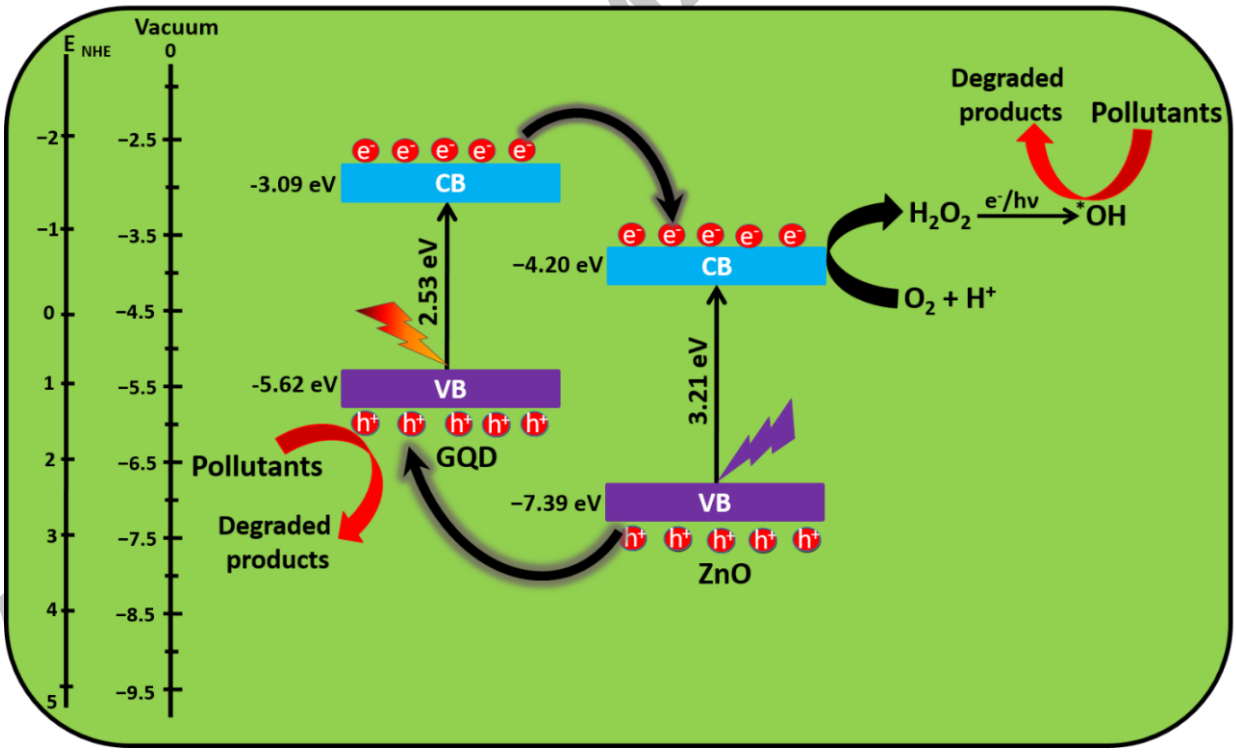


**Scheme 1.** Schematic illustration of energy band diagram and a proposed mechanism of the charge carrier transitions in ZnO-GQD heterojunction towards photocatalytic pollutant degradation under natural sunlight irradiation.

**Table 1.** Comparison of photocatalytic activities of ZnO and GQD based nanocomposites for degradation of various pollutants.

| Sl. No. | Photocatalyst | Synthesis Route | Irradiation Source | Pollutant and Concentration | $T_{completion}$ | Ref. |
|---|---|---|---|---|---|---|
| 1 | GQD | Pyrolyzing citric acid method | visible light | NF (20 mg $L^{-1}$) | 110 min | [49] |
| 2 | GQD-$TiO_2$ | Molecular fusion and hydrothermal | 350 W Xe lamp | MO (10 mg $L^{-1}$) | 120 min | [36] |
| 3 | GQD-$TiO_2$ NTA | Impregnation method | UV light (6 W) | MB (20 mM) | 180 min | [54] |
| 4 | ZnO-CQD | Hydrothermal | xenon arc lamp | Rh B ($5 \times 10^{-6}$ M) | 105 min | [55] |
| 5 | ZnO-GR | Solvothermal | halogen lamp | MB (20 mg $L^{-1}$) | 90 min | [56] |
| 6 | ZnO-GO | Chemical route | xenon arc lamp | Cv | 80 min | [57] |
| 7 | ZnO-RGO | Microwave assisted | 500 W Hg lamp | MB (5 mg $L^{-1}$) | 260 min | [58] |
| 8 | GQD-ZnO | Hydrothermal | Sunlight | MB (1.0 X $10^{-5}$ M) | 70 min | This work |

GQD-graphene quantum dots; NF- new fuchsin; NTA- nanotube arrays; MO-methyl orange; MB-methylene blue; CQD-carbon quantum dots; Rh B- rhodamine b; Cv- crystal violet; GR-graphene; GO-graphene oxide; RGO-reduced graphene oxide.

### 3.7. Reusability of the photocatalyst

The reusability of best catalyst (ZGQD2) was investigated for four recycles of photocatalytic degradation of CZ and the corresponding results are presented in Figure 12(a). After each catalytic recycle, the catalyst was recovered by centrifugation, washed with deionized water to remove residual CZ content and finally dried before using for next cycle. All recycling experiments were carried out under same experimental conditions as that of first cycle. It can be seen clearly from Figure 12 (a) that no significant loss in the photocatalytic activity was observed even after 4 recycles and still the removal rate of CZ was 91%. This small loss of photocatalytic activity (from 95% to 91%) after four recycles could be attributed to the loss of photocatalyst during each recovery process. Hence, these results demonstrate ZGQD2 heterojunction as a stable photocatalyst for the removal of organic pollutants from water. Moreover, the recycled ZGQD2 heterojunction was characterized by XRD to confirm its crystal

structure and the obtained patterns are depicted in Figure 12 (b) alongside with the heterojunction before the photocatalysis process. All the characteristic diffraction peaks of ZGQD2 heterojunction have been retained in the recycled catalyst, which confirms its excellent photostability.

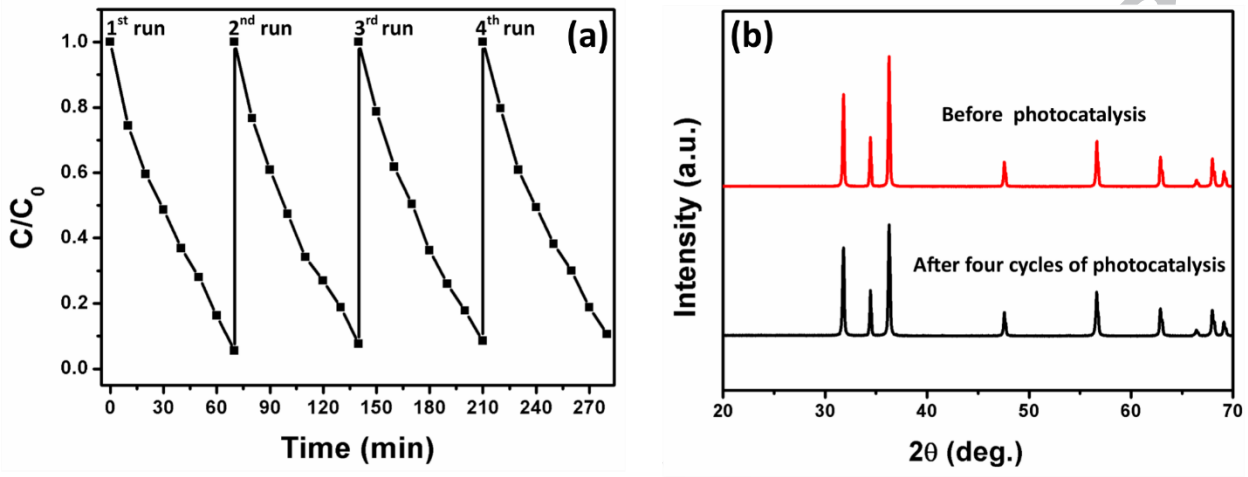


**Figure 12.** (a) Recyclability of ZGQD2 heterojunction for photocatalytic degradation of CZ and (b) XRD patterns of ZGQD2 heterojunction before and after photocatalytic reaction.

## 4. Conclusions

In this detailed study, we have designed and developed GQD loaded ZnO NR heterojunctions by using a facile hydrothermal synthesis method and demonstrated them as effective photocatalysts for removal of organic pollutants (MB and CZ) in water using sunlight. TEM images showed the uniform decoration of GQD over ZnO NR to form heterojunction with intimate interfacial contacts. Moreover, XPS and UV-visible DRS studies indicate the strong interactions between ZnO and GQD, and the extended light absorption of heterojunction towards visible region, beyond the fundamental absorption of ZnO. Upon sunlight irradiation, ZnO-GQD heterojunctions exhibit remarkably enhanced photocatalytic activity for degradation of colored (MB) and colorless (CZ) pollutants as compared to bare ZnO and GQD. Heterojunction with 2wt% of GQD showed the highest photocatalytic activity, which was eight times higher than bare ZnO. The superior photocatalytic performance of ZnO-GQD heterojunctions could be attributed to the enhanced solar spectrum utilization, effective separation of photoinduced electron-hole pairs across the ZnO-GQD interface, facilitated

electrons transfer and high specific surface area with abundant reaction sites. Active species trapping experiments reveals the generation of $^{*}OH$ and $h^{+}$ during photocatalytic reaction, which are responsible for the degradation of the organic pollutants. Hence, present study provides new insights into development of GQD and semiconductors based heterojunctions as efficient photocatalysts for water purification.

## Acknowledgements

We are thankful to Advanced Materials Research Centre (AMRC), IIT Mandi for the characterization facilities. VK acknowledges the financial support from Department of Science and Technology (DST), India under SERB Young Scientist Scheme (YSS/2014/000456/CS). SK acknowledges research fellowship from University Grants Commission (UGC), India.

**References**

[1] S. Kumar, N.L. Reddy, H.S. Kushwaha, A. Kumar, M.V. Shankar, K. Bhattacharyya, A. Halder, V. Krishnan, Efficient Electron Transfer across ZnO-MoS2-RGO Heterojunction for Remarkably Enhanced Sunlight Driven Photocatalytic Hydrogen Evolution, ChemSusChem, 10 (2017) 3588-3603.

[2] S. Kumar, A. Kumar, A. Bahuguna, V. Sharma, V. Krishnan, Two-dimensional carbon-based nanocomposites for photocatalytic energy generation and environmental remediation applications, Beilstein Journal of Nanotechnology, 8 (2017) 1571-1600.

[3] X. Chen, N. Li, Z. Kong, W.-J. Ong, X. Zhao, Photocatalytic fixation of nitrogen to ammonia: state-of-the-art advancements and future prospects, Materials Horizons, (2018) DOI: 10.1039/C7MH00557A.

[4] I.K. Konstantinou, T.A. Albanis, TiO 2-assisted photocatalytic degradation of azo dyes in aqueous solution: kinetic and mechanistic investigations: a review, Applied Catalysis B: Environmental, 49 (2004) 1-14.

[5] R.G. Nair, S. Mazumdar, B. Modak, R. Bapat, P. Ayyub, K. Bhattacharyya, The role of surface O-vacancies in the photocatalytic oxidation of Methylene Blue by Zn-doped TiO 2: A

Mechanistic approach, Journal of Photochemistry and Photobiology A: Chemistry, 345 (2017) 36-53.

[6] M.-Q. Yang, N. Zhang, M. Pagliaro, Y.-J. Xu, Artificial photosynthesis over graphene–semiconductor composites. Are we getting better?, Chemical Society Reviews, 43 (2014) 8240-8254.

[7] A. Kudo, Y. Miseki, Heterogeneous photocatalyst materials for water splitting, Chemical Society Reviews, 38 (2009) 253-278.

[8] F. Chen, Q. Yang, X. Li, G. Zeng, D. Wang, C. Niu, J. Zhao, H. An, T. Xie, Y. Deng, Hierarchical assembly of graphene-bridged Ag 3 PO 4/Ag/BiVO 4 (040) Z-scheme photocatalyst: An efficient, sustainable and heterogeneous catalyst with enhanced visible-light photoactivity towards tetracycline degradation under visible light irradiation, Applied Catalysis B: Environmental, 200 (2017) 330-342.

[9] X. Chen, S. Shen, L. Guo, S.S. Mao, Semiconductor-based photocatalytic hydrogen generation, Chemical Reviews, 110 (2010) 6503-6570.

[10] S. Sakthivel, B. Neppolian, M. Shankar, B. Arabindoo, M. Palanichamy, V. Murugesan, Solar photocatalytic degradation of azo dye: comparison of photocatalytic efficiency of ZnO and TiO 2, Solar Energy Materials and Solar Cells, 77 (2003) 65-82.

[11] J. Yang, C. Chen, H. Ji, W. Ma, J. Zhao, Mechanism of TiO2-assisted photocatalytic degradation of dyes under visible irradiation: photoelectrocatalytic study by TiO2-film electrodes, The Journal of Physical Chemistry B, 109 (2005) 21900-21907.

[12] V. Sharma, S. Kumar, V. Krishnan, Homogeneously embedded Pt nanoclusters on amorphous titania matrix as highly efficient visible light active photocatalyst material, Materials Chemistry and Physics, 179 (2016) 129-136.

[13] W.-J. Ong, L.-L. Tan, Y.H. Ng, S.-T. Yong, S.-P. Chai, Graphitic carbon nitride (g-C3N4)-based photocatalysts for artificial photosynthesis and environmental remediation: are we a step closer to achieving sustainability?, Chem. Rev, 116 (2016) 7159-7329.

[14] D. Zeng, W.-J. Ong, H. Zheng, M. Wu, Y. Chen, D.-L. Peng, M.-Y. Han, Ni 12 P 5 nanoparticles embedded into porous gC 3 N 4 nanosheets as a noble-metal-free hetero-structure

photocatalyst for efficient H 2 production under visible light, Journal of Materials Chemistry A, 5 (2017) 16171-16178.

[15] W.-J. Ong, L.K. Putri, Y.-C. Tan, L.-L. Tan, N. Li, Y.H. Ng, X. Wen, S.-P. Chai, Unravelling charge carrier dynamics in protonated g-C3N4 interfaced with carbon nanodots as co-catalysts toward enhanced photocatalytic CO2 reduction: A combined experimental and first-principles DFT study, Nano Research, 10 (2017) 1673-1696.

[16] W.-J. Ong, 2D/2D graphitic carbon nitride (g-C3N4) heterojunction nanocomposites for photocatalysis: Why does face-to-face interface matter?, Frontiers in Materials, 4 (2017) 11.

[17] M. Agrawal, S. Gupta, A. Pich, N.E. Zafeiropoulos, M. Stamm, A Facile Approach to Fabrication of ZnO− TiO2 Hollow Spheres, Chemistry of Materials, 21 (2009) 5343-5348.

[18] C.-p. Tso, C.-m. Zhung, Y.-h. Shih, Y.-M. Tseng, S.-c. Wu, R.-a. Doong, Stability of metal oxide nanoparticles in aqueous solutions, Water Science and Technology, 61 (2010) 127-133.

[19] V. Sharma, S. Kumar, V. Krishnan, Clustered Au on TiO2 Snowman-Like Nanoassemblies for Photocatalytic Applications, ChemistrySelect, 1 (2016) 2963-2970.

[20] Y. Li, W. Xie, X. Hu, G. Shen, X. Zhou, Y. Xiang, X. Zhao, P. Fang, Comparison of dye photodegradation and its coupling with light-to-electricity conversion over TiO2 and ZnO, Langmuir, 26 (2009) 591-597.

[21] T. Tsuzuki, Abnormal Transmittance of Refractive-Index-Modified ZnO/Organic Hybrid Films, Macromolecular Materials and Engineering, 293 (2008) 109-113.

[22] S. Kumar, V. Sharma, K. Bhattacharyya, V. Krishnan, Synergetic effect of MoS 2–RGO doping to enhance the photocatalytic performance of ZnO nanoparticles, New Journal of Chemistry, 40 (2016) 5185-5197.

[23] P. Pawinrat, O. Mekasuwandumrong, J. Panpranot, Synthesis of Au–ZnO and Pt–ZnO nanocomposites by one-step flame spray pyrolysis and its application for photocatalytic degradation of dyes, Catalysis Communications, 10 (2009) 1380-1385.

[24] B. Li, T. Liu, Y. Wang, Z. Wang, ZnO/graphene-oxide nanocomposite with remarkably enhanced visible-light-driven photocatalytic performance, Journal of Colloid and Interface Science, 377 (2012) 114-121.

[25] X. An, C.Y. Jimmy, Graphene-based photocatalytic composites, RSC Advances, 1 (2011) 1426-1434.

[26] S. Kumar, V. Sharma, K. Bhattacharyya, V. Krishnan, N-doped ZnO–MoS 2 binary heterojunctions: the dual role of 2D MoS 2 in the enhancement of photostability and photocatalytic activity under visible light irradiation for tetracycline degradation, Materials Chemistry Frontiers, 1 (2017) 1093--1106.

[27] Z. Wang, B. Huang, Y. Dai, X. Qin, X. Zhang, P. Wang, H. Liu, J. Yu, Highly photocatalytic ZnO/In2O3 heteronanostructures synthesized by a coprecipitation method, The Journal of Physical Chemistry C, 113 (2009) 4612-4617.

[28] S. Balachandran, M. Swaminathan, Facile fabrication of heterostructured Bi2O3–ZnO photocatalyst and its enhanced photocatalytic activity, The Journal of Physical Chemistry C, 116 (2012) 26306-26312.

[29] W. Wu, S. Zhang, X. Xiao, J. Zhou, F. Ren, L. Sun, C. Jiang, Controllable synthesis, magnetic properties, and enhanced photocatalytic activity of spindlelike mesoporous α-Fe2O3/ZnO core–shell heterostructures, ACS Applied Materials & Interfaces, 4 (2012) 3602-3609.

[30] S. Mukhopadhyay, I. Mondal, U. Pal, P.S. Devi, Fabrication of hierarchical ZnO/CdS heterostructured nanocomposites for enhanced hydrogen evolution from solar water splitting, Physical Chemistry Chemical Physics, 17 (2015) 20407-20415.

[31] P. Kundu, P.A. Deshpande, G. Madras, N. Ravishankar, Nanoscale ZnO/CdS heterostructures with engineered interfaces for high photocatalytic activity under solar radiation, Journal of Materials Chemistry, 21 (2011) 4209-4216.

[32] S. Kumar, R. Sharma, V. Sharma, G. Harith, V. Sivakumar, V. Krishnan, Role of RGO support and irradiation source on the photocatalytic activity of CdS–ZnO semiconductor nanostructures, Beilstein Journal of Nanotechnology, 7 (2016) 1684-1697.

[33] A. Kumar, S. Kumar, A. Bahuguna, A. Kumar, V. Sharma, V. Krishnan, Recyclable, Bifunctional Composites of Perovskite Type N-CaTiO3 and Reduced Graphene Oxide as an Efficient Adsorptive Photocatalyst for Environmental Remediation, Materials Chemistry Frontiers, 1 (2017) 2391--2404.

[34] A. Raja, A.s. Montoya− Castillo, J. Zultak, X.-X. Zhang, Z. Ye, C. Roquelet, D.A. Chenet, A.M. van der Zande, P. Huang, S. Jockusch, Energy transfer from quantum dots to graphene and MoS2: The role of absorption and screening in two-dimensional materials, Nano Letters, 16 (2016) 2328-2333.

[35] J.-P. Zou, L.-C. Wang, J. Luo, Y.-C. Nie, Q.-J. Xing, X.-B. Luo, H.-M. Du, S.-L. Luo, S.L. Suib, Synthesis and efficient visible light photocatalytic H 2 evolution of a metal-free gC 3 N 4/graphene quantum dots hybrid photocatalyst, Applied Catalysis B: Environmental, 193 (2016) 103-109.

[36] D. Pan, J. Jiao, Z. Li, Y. Guo, C. Feng, Y. Liu, L. Wang, M. Wu, Efficient separation of electron–hole pairs in graphene quantum dots by TiO2 heterojunctions for dye degradation, ACS Sustainable Chemistry & Engineering, 3 (2015) 2405-2413.

[37] S. Min, J. Hou, Y. Lei, X. Ma, G. Lu, Facile one-step hydrothermal synthesis toward strongly coupled TiO 2/graphene quantum dots photocatalysts for efficient hydrogen evolution, Applied Surface Science, 396 (2017) 1375-1382.

[38] M. Yan, Y. Hua, F. Zhu, W. Gu, J. Jiang, H. Shen, W. Shi, Fabrication of nitrogen doped graphene quantum dots-BiOI/MnNb 2 O 6 pn junction photocatalysts with enhanced visible light efficiency in photocatalytic degradation of antibiotics, Applied Catalysis B: Environmental, 202 (2017) 518-527.

[39] J. Liu, H. Xu, Y. Xu, Y. Song, J. Lian, Y. Zhao, L. Wang, L. Huang, H. Ji, H. Li, Graphene quantum dots modified mesoporous graphite carbon nitride with significant enhancement of photocatalytic activity, Applied Catalysis B: Environmental, 207 (2017) 429-437.

[40] P. Sudhagar, I. Herraiz-Cardona, H. Park, T. Song, S.H. Noh, S. Gimenez, I.M. Sero, F. Fabregat-Santiago, J. Bisquert, C. Terashima, Exploring Graphene Quantum Dots/TiO 2 interface in photoelectrochemical reactions: Solar to fuel conversion, Electrochimica Acta, 187 (2016) 249-255.

[41] C.X. Guo, Y. Dong, H.B. Yang, C.M. Li, Graphene Quantum Dots as a Green Sensitizer to Functionalize ZnO Nanowire Arrays on F-Doped SnO2 Glass for Enhanced Photoelectrochemical Water Splitting, Advanced Energy Materials, 3 (2013) 997-1003.

[42] X. Sun, C. Zhou, M. Xie, H. Sun, T. Hu, F. Lu, S.M. Scott, S.M. George, J. Lian, Synthesis of ZnO quantum dot/graphene nanocomposites by atomic layer deposition with high lithium storage capacity, Journal of Materials Chemistry A, 2 (2014) 7319-7326.

[43] D.I. Son, B.W. Kwon, D.H. Park, W.-S. Seo, Y. Yi, B. Angadi, C.-L. Lee, W.K. Choi, Emissive ZnO-graphene quantum dots for white-light-emitting diodes, Nature Nanotechnology, 7 (2012) 465-471.

[44] Z. Zang, X. Zeng, J. Du, M. Wang, X. Tang, Femtosecond laser direct writing of microholes on roughened ZnO for output power enhancement of InGaN light-emitting diodes, Optics letters, 41 (2016) 3463-3466.

[45] M. Dutta, S. Sarkar, T. Ghosh, D. Basak, ZnO/graphene quantum dot solid-state solar cell, The Journal of Physical Chemistry C, 116 (2012) 20127-20131.

[46] N. Suzuki, Y. Wang, P. Elvati, Z.-B. Qu, K. Kim, S. Jiang, E. Baumeister, J. Lee, B. Yeom, J.H. Bahng, Chiral graphene quantum dots, ACS Nano, 10 (2016) 1744-1755.

[47] Y. Li, Z. Wu, D. Du, H. Dong, D. Shi, Y. Li, A graphene quantum dot (GQD) nanosystem with redox-triggered cleavable PEG shell facilitating selective activation of the photosensitiser for photodynamic therapy, RSC Advances, 6 (2016) 6516-6522.

[48] M. Hassan, E. Haque, K.R. Reddy, A.I. Minett, J. Chen, V.G. Gomes, Edge-enriched graphene quantum dots for enhanced photo-luminescence and supercapacitance, Nanoscale, 6 (2014) 11988-11994.

[49] M. Roushani, M. Mavaei, H.R. Rajabi, Graphene quantum dots as novel and green nano-materials for the visible-light-driven photocatalytic degradation of cationic dye, Journal of Molecular Catalysis A: Chemical, 409 (2015) 102-109.

[50] D. Pan, C. Xi, Z. Li, L. Wang, Z. Chen, B. Lu, M. Wu, Electrophoretic fabrication of highly robust, efficient, and benign heterojunction photoelectrocatalysts based on graphene-quantum-dot sensitized TiO 2 nanotube arrays, Journal of Materials Chemistry A, 1 (2013) 3551-3555.

[51] C. Chen, Y. Lu, H. He, M. Xiao, Z. Wang, L. Chen, Z. Ye, Violet emission in ZnO nanorods treated with high-energy hydrogen plasma, ACS Applied Materials & Interfaces, 5 (2013) 10274-10279.

[52] J. Shen, Y. Zhu, X. Yang, C. Li, Graphene quantum dots: emergent nanolights for bioimaging, sensors, catalysis and photovoltaic devices, Chemical communications, 48 (2012) 3686-3699.

[53] Y. Xu, M.A. Schoonen, The absolute energy positions of conduction and valence bands of selected semiconducting minerals, American Mineralogist, 85 (2000) 543-556.

[54] B.K. Gupta, G. Kedawat, Y. Agrawal, P. Kumar, J. Dwivedi, S. Dhawan, A novel strategy to enhance ultraviolet light driven photocatalysis from graphene quantum dots infilled TiO 2 nanotube arrays, RSC Advances, 5 (2015) 10623-10631.

[55] H. Bozetine, Q. Wang, A. Barras, M. Li, T. Hadjersi, S. Szunerits, R. Boukherroub, Green chemistry approach for the synthesis of ZnO–carbon dots nanocomposites with good photocatalytic properties under visible light, Journal of Colloid and Interface Science, 465 (2016) 286-294.

[56] M. Ahmad, E. Ahmed, Z. Hong, J. Xu, N. Khalid, A. Elhissi, W. Ahmed, A facile one-step approach to synthesizing ZnO/graphene composites for enhanced degradation of methylene blue under visible light, Applied Surface Science, 274 (2013) 273-281.

[57] S. Ameen, M.S. Akhtar, H.-K. Seo, H.S. Shin, Advanced ZnO–graphene oxide nanohybrid and its photocatalytic applications, Materials Letters, 100 (2013) 261-265.

[58] T. Lv, L. Pan, X. Liu, T. Lu, G. Zhu, Z. Sun, Enhanced photocatalytic degradation of methylene blue by ZnO-reduced graphene oxide composite synthesized via microwave-assisted reaction, Journal of Alloys and Compounds, 509 (2011) 10086-10091.

## Research highlights

* Heterojunctions with ZnO nanorods decorated with GQD were prepared by facile hydrothermal method

* ZnO with 2wt% of GQD exhibits highest photocatalytic activity for removal of pollutants

* Enhanced light absorption and efficient separation of photoinduced charge carriers boosts the photoactivity

* Plausible mechanism for superior photocatalytic activity has been proposed based on the investigations

**Graphical abstract**